Quantitative Magnetization Transfer Characteristics of the Human Cervical Spinal Cord In Vivo: Application to Adrenomyeloneuropathy

Seth A. Smith,[1,2*] Xavier Golay,[1,3] Ali Fatemi,[2,4] Asif Mahmood,[2,4] Gerald V. Raymond,[4] Hugo W. Moser,[†] Peter C.M. van Zijl,[1,2] and Greg J. Stanisz[5,6]

Magnetization transfer (MT) imaging has assessed myelin integrity in the brain and spinal cord; however, quantitative MT (qMT) has been confined to the brain or excised tissue. We characterized spinal cord tissue with qMT in vivo, and as a first application, qMT-derived metrics were examined in adults with the genetic disorder Adrenomyeloneuropathy (AMN). AMN is a progressive disease marked by demyelination of the white matter tracts of the cervical spinal cord, and a disease in which conventional MRI has been limited. MT data were acquired at 1.5 Tesla using 10 radiofrequency offsets at one power in the cervical cord at C2 in 6 healthy volunteers and 9 AMN patients. The data were fit to a two-pool MT model and the macromolecular fraction (M_{ob}), macromolecular transverse relaxation time (T_{2b}) and the rate of MT exchange (R) for lateral and dorsal column white matter and gray matter were calculated. M_{ob} for healthy volunteers was: WM = 13.9 ± 2.3%, GM = 7.9 ± 1.5%. In AMN, dorsal column M_{ob} was significantly decreased ($P < 0.03$). T_{2b} for volunteers was: 9 ± 2 μs and the rate of MT exchange (R) was: WM = 56 ± 11 Hz, GM = 67 ± 12 Hz. Neither T_{2b} nor R showed significant differences between healthy and diseased cords. Comparisons are made between qMT, and conventional MT acquisitions. Magn Reson Med 61:22–27, 2009. © 2008 Wiley-Liss, Inc.

Key words: magnetization transfer; spinal cord; MT exchange; adrenomyeloneuropathy

MRI has been established as a useful tool in determining and monitoring white matter pathology in the human body. Standard MR methodology, such as longitudinal (T_1) and transverse (T_2) relaxation time and diffusion measurements have been shown to be sensitive to the presence of abnormal tissue microstructure such as dys/demyelination, axonal loss, inflammation, and gliosis. However, in the central nervous system (CNS), each of these experiments are derived from measurements of the of bulk water and reflect changes in molecular mobility or water density associated with tissue microstructure. Alternatively, it has been noticed that many white matter (WM) pathologies exhibit reorganization/changes in macromolecular constitution and that these changes are poorly reflected in standard relaxation or diffusion measurements. To assess these changes, two experimental techniques are often used: magnetic resonance spectroscopy (MRS) and magnetization transfer (MT).

MT imaging indirectly measures the interaction between mobile water protons and protons residing within, or intimately associated with macromolecules of the CNS. It is hypothesized that the bulk of the MT effect comes from the abundant hydroxyl moieties of the glycolipid head group of fatty acids (sphyngosine, cerebroside) comprising the myelin sheets and are the most prevalent macromolecules in WM (1). Therefore, MT imaging of the CNS may reveal early changes in WM not detectable otherwise by conventional imaging.

The magnitude of the MT effect is generally characterized by the MT ratio (MTR) which is defined as (2):

$$MTR(\Delta\omega) = 1 - \frac{S(\Delta\omega)}{S_0} \quad [1]$$

where $S(\Delta\omega)$ is the signal in the presence of the MT saturation pulse at offset frequency, $\Delta\omega$, and S_o is the signal in the absence of RF irradiation. Single frequency MTR imaging has been useful in assessing tissue pathology (3–10), but because it depends on experimental parameters and tissue relaxation, it is not specific. More rigorous, quantitative methods have been developed which consist of collecting MT-weighted data at multiple offset frequencies and/or RF saturation (so-called MT z-spectrum) (11) powers and using mathematical models to extract intrinsic characteristics of the MT process (12–16). A two-pool model with exchange can be used to reveal metrics such as the fraction of macromolecular protons (M_{ob}), the rate of MT exchange (R), and the transverse relaxation time of macromolecular spins (T_{2b}) and is generally termed quantitative MT (qMT). Specifically, M_{ob} has been shown to scale with the myelin content whereas R and T_{2b} may reflect changes within myelin lipid structure (15).

qMT has been largely used to assess brain tissue in vivo (14,16), but data on many tissues ex vivo (human and animal) (12,13,15) are also available. To date, qMT has not been used to study the spinal cord in vivo, because the spinal cord offers a difficult environment to apply techniques that have been designed for the brain. High resolution is necessary to distinguish gray and white matter, and

[1]Russell H. Morgan Department of Radiology and Radiological Science, Johns Hopkins University School of Medicine, Baltimore, Maryland.

[2]F.M. Kirby Research Center for Functional Brain Imaging Kennedy Krieger Institute, Baltimore, Maryland.

[3]Laboratory of Molecular Imaging, Singapore Bioimaging Consortium, and Department of Neuroradiology, National Neuroscience Institute, Singapore.

[4]Department of Neurogenetics, Kennedy Krieger Institute, Baltimore, Maryland.

[5]Imaging Research, Sunnybrook Health Sciences Centre, Toronto, Canada.

[6]Department of Medical Biophysics, University of Toronto, Toronto, Canada.

Grant sponsor: NIH/NCRR; Grant number: RR015241.

*Correspondence to: Seth A. Smith, F.M. Kirby Research Center for Functional Brain Imaging, Kennedy Krieger Institute, 707 N. Broadway, Baltimore, MD 21205. E-mail: smith@mri.jhu.edu

†Dr. Moser is deceased.

Received 13 June 2008; revised 25 August 2008; accepted 25 August 2008.

DOI 10.1002/mrm.21827

Published online in Wiley InterScience (www.interscience.wiley.com).

the spinal cord itself is small and mobile. However, the spinal cord is an important structure anatomically serving as a conduit of information from the brain to the extremities, and is affected in some of the most devastating disorders of the CNS. Thus, an accurate assessment of its physiology would be paramount to understanding the nature of diseases that afflict the CNS.

To evaluate qMT in the spinal cord, we examined healthy volunteers and patients diagnosed with the genetic disorder, Adrenomyeloneuropathy (AMN). AMN is the adult form of X-linked Adrenoleukodystrophy (X-ALD), a disorder of the peroxisomal beta-oxidation of very long chain fatty acids. It mostly affects men in their early 20s and to a lesser degree, women, heterozygous for the X-ALD gene, later in life (17,18). Pathologically, AMN presents as a primary, retrograde, distal axonopathy with secondary demyelination of the dorsal columns in the cervical cord and the thoraco-lumbar lateral columns (18). In contrast to multiple sclerosis, AMN does not have an overt inflammatory component, and conventional (T_1- and T_2-weighted) MRI has shown no significant changes other than cord atrophy late in the disease. However, it is suspected that AMN is the result of accumulation of fatty acids in spinal cord, resulting in the structural destabilization of myelin lipid content leading to myelin breakdown (18). We have shown previously that MT-weighted imaging is sensitive to cord pathology in the cervical dorsal columns in AMN patients (19,20). Here, we apply the more rigorous, quantitative approach (qMT).

Our goal was to apply a two-pool model of MT to spinal cord tissue in vivo, in healthy controls and patients with AMN. In this work, fitted values for the rate of MT exchange (R), transverse relaxation time of macromolecular spins (T_{2b}), and macromolecular pool fraction (M_{ob}) are reported for dorsal and lateral column white matter (WM), as well as dorsolateral gray matter found in the upper cervical spinal cord (C2). Results are obtained by fitting MT z-spectra from 1 to 64 kHz offset to a two-pool model of MT (14).

MATERIALS AND METHODS

Some of the patients and imaging methodologies presented here overlap with two previous manuscripts (19,20). This protocol was approved by the local institutional review board, and signed, informed consent was obtained before examination. The study participants were six healthy volunteers (three male, three female; mean age, 28.8 ± 5.6 years), four males (mean age, 37 ± 12 years) diagnosed with AMN (mean EDSS = 4.3; range = 3–5), and five females (mean age, 46 ± 10 years) heterozygous for the X-ALD gene (mean EDSS = 2.7; range = 1–5).

The full details of the scanning protocol are given elsewhere (19,20). All MRI scans were acquired using a Philips Intera 1.5 Tesla (T; Philips Medical Systems, Best, The Netherlands) MRI system with transmit body coil and a two-element receive surface coil. MT-weighted images were obtained between C1 and C3 using a three-dimensional gradient echo (TR/TE/α = 50 ms/12 ms/7°), with a five-lobed, sinc-shaped MT prepulse (pulse duration = 15 ms, peak B_1 = 14.5 μT), and 10 radiofrequency (RF) offset frequencies logarithmically sampled between 1 and 64 kHz. A reference scan with no MT irradiation was also acquired.

Region of Interest Selection and Fitting Methodology

Because AMN is a diffuse disease and pathology extends over many levels of the cord, a single level was judged to be a sufficient representation of a much larger segment of the spinal cord. Thus, 4 slices at 1.5 mm thick and centered at C2 were further examined. Regions of interest (ROIs) were selected in the lateral and dorsal column WM and dorsolateral horn gray matter (GM). Care was taken to minimize visual partial volume contacts with neighboring tissues; however, due to the small size of the spinal cord, partial volume effects are unavoidable. The average number of voxels in each ROI was 60.

The MT data were analyzed using a two-pool model of MT exchange using the mathematical formalism proposed by Sled and Pike (14, 26) and further adapted by Portnoy and Stanisz (21, 22). This model decomposes the MT pulse sequence into a series of stages: (i) constant-amplitude, off-resonance irradiation of semisolid proton pool, (ii) periods of free precession and, (iii) instantaneous saturation of the free water pool. In each of these cases, the modified Bloch equations including exchange bear constant coefficients and can be solved analytically for both steady and transient states. Furthermore, the transverse and longitudinal components of magnetization are decoupled, and for simplicity, only the longitudinal components of magnetization were modeled as the transverse components were assumed to disappear through relaxation and spoiling. Using these approximations analytical expressions exist for the longitudinal magnetization throughout each stage.

To describe the propagation of the magnetization through the sequence, the endpoint values of each stage were used as initial conditions for the next. Finally, a closed form solution was obtained, by imposing the condition that a sufficient number RF pulses were applied to ensure attainment of a pulsed steady state (i.e., the magnetization behaves periodically with TR). The resultant analysis yielded the semisolid pool fraction, M_{ob}, the transverse relaxation time of macromolecules, T_{2b}, and the rate of MT exchange, R as well as uncertainties associated with each MT parameter (22).

Data Comparison

In healthy spinal cord tissue, it is not well known whether or not WM columns will differ from each other and, therefore, we compared the mean of each derived metric in lateral column with dorsal column WM in healthy controls. Finally as a test for the sensitivity of qMT derived parameters, we compared the mean of each metric for the dorsal and lateral column WM between patients and controls. All comparisons were performed using Wilcoxon rank sum test, as the number of entries was insufficient to warrant t-test.

RESULTS

Figure 1 shows MT-weighted images obtained in a healthy volunteer (Fig. 1a) and a patient with AMN (Fig. 1b) at the

level of C2 as a function of offset frequency. In Figure 1A, excellent contrast between GM and WM can be appreciated at higher offset frequencies, while at lower offset frequencies, the tissues are equally saturated such that no GM/WM contrast can be observed. The final image in panel a shows a representation of the ROIs that were selected for further analysis in all subjects: lateral columns (red), dorsal column (blue), and dorsolateral horn GM (yellow). In Figure 1b, a representative data set from a mildly afflicted AMN male is presented. Note that in this patient, little cord atrophy is evident, however dorsal column hyperintensities (red arrow) appear in each image at offsets > 1 kHz.

Figure 2 shows experimental data and fits to the dorsal column MT z-spectra of the patient (blue) and healthy volunteer (black) presented in Figure 1. It should be pointed out that for most offset frequencies the z-spectrum in the AMN patient (triangle) is elevated relative to the healthy control (square). This is not entirely surprising and is consistent with the tissue pathology in the AMN patients.

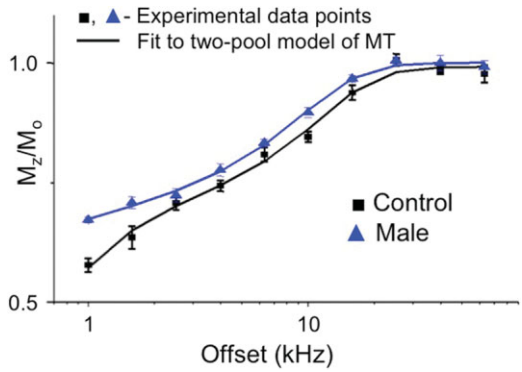

FIG. 2. Acquired z-spectra and fitted results for the healthy control (black) and AMN patient (blue) presented in Figure 1. Solid lines indicate qMT fit result, while data points represent the mean normalized signal intensity in the dorsal column. Similarly to Figure 1, the dorsal column signal intensity in the AMN patient is elevated for all offset frequencies with respect to the control.

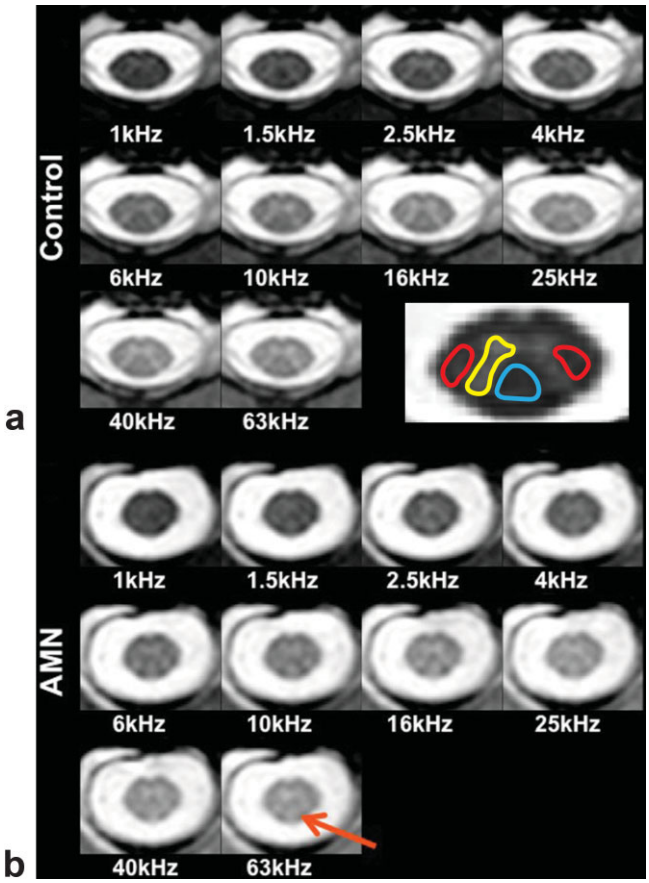

FIG. 1. MT-weighted images taken at the level of C2 as a function of offset frequency. **a**: Healthy control. Excellent discrimination between gray and white matter can be appreciated at all offsets greater than 4 kHz. The contrast is such that tissue with a large MT effect (e.g., white matter) is dark relative to GM and CSF (brightest). The image on the bottom right reflects the placement of ROIs used for qMT analysis: lateral columns (red), dorsal column (blue) white matter, and dorsolateral horn (yellow) gray matter. **b**: Mildly affected AMN male. At all offsets greater than 1 kHz, tissue hyperintensity in the dorsal column (red arrow) is observed. It should be noted that the dorsal column is the principle site of pathology (18) in the cervical level of AMN patients.

In Figure 3, bar graphs show mean qMT-derived metrics over all patients and controls. Each bar color represents the mean of the metric of interest over each class of subjects (control, black; X-ALD female heterozygote, red; AMN male, blue). Individual patient data are given in Table 1.

In healthy volunteers, the mean rate of MT exchange, R, in WM (averaged over dorsal and lateral) was 56 ± 11 Hz and GM $= 67 \pm 12$ Hz. While not significant, this demonstrates a slight disparity in the rate of MT exchange between WM and GM in the cord. Comparisons between control lateral and dorsal column WM rate of MT exchange revealed no significant differences ($P = 0.5$); however, analysis of the MT exchange rate between lateral column WM and GM showed a significant difference (lateral column WM: 52 ± 8 Hz vs. GM: 67 ± 12 Hz $P < 0.03$). No significant difference was observed between patients and healthy controls.

The mean white matter macromolecular fraction, M_{ob} in healthy controls was $14 \pm 2\%$. In GM, the mean $M_{ob} = 8 \pm 2\%$. Due to the high degree of partial volume effects in GM measurements, we expect the GM value to be slightly bloated; however, these values coincide with reports of cerebral deep GM M_{ob} (14). M_{ob} was statistically equivalent between lateral and dorsal column WM in healthy controls, and both WM columns showed a statistical elevation in M_{ob} when compared with GM ($P = 0.002$). In the AMN patients, the lateral columns and GM showed no significant difference compared with controls. However, in the dorsal column, M_{ob} in X-ALD exhibited a trend toward significance ($P = 0.1$) and AMN males showed significant decrease in M_{ob} ($P < 0.03$) when compared with controls. No disparity was observed between AMN phenotypes.

The mean macromolecular relaxation time, T_{2b} across all columns in healthy volunteers was 9 ± 2 μs for WM and GM. For lateral, dorsal column WM, and GM, there was no significant difference between any of the patient classes and controls. However, as seen in Figure 3, large variabil-

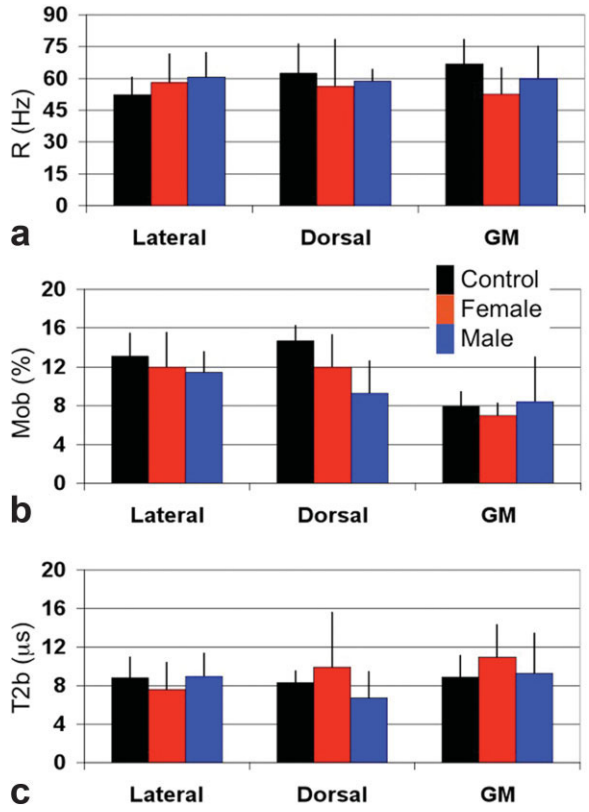

FIG. 3. Mean qMT metrics for controls (black), X-ALD females (red) and AMN males (blue) for each of the dorsal and lateral columns and dorsolateral horn gray matter. **a**: Rate of MT exchange (R) in Hz. R is approximately the same for all volunteers and subjects with AMN for each of the columns and GM. **b**: Fraction of bound spins (M_{ob}). Mob is seen to decrease in the dorsal column, which is the principle site of pathology, in AMN patients as compared to healthy controls. Similarly, a significant difference between WM and GM M_{ob} can be appreciated. **c**: Transverse relaxation time of bound spins (T_{2b}). T_{2b} is approximately the same for all subjects studied. However, the large variability in T_{2b} for the X-ALD females in the dorsal column could be a result of hydrophobic interactions with bulk water caused by increase in very long chain fatty acid incorporation into the myelin membrane.

ity was observed in the dorsal column T_{2b} values for the X-ALD patients (range, 3.8 μs to 16.5 μs) and is shown in detail in Table 1.

Of note is the quality of the fits for volunteers and patients. Chi-squared analysis revealed that the normalized χ^2 for all fits was on average 1.3 and not exceeding 1.6 indicating a strong degree of association between data and fit. The average errors in each of the fitted parameters did not exceed 7% error at the 95th percent confidence level.

DISCUSSION

We describe qMT measurements of the human spinal cord in vivo. As a first test, we applied this technique to Adrenomyeloneuropathy, a disease of the spinal cord with no conventional imaging maker for progression. Dorsal and lateral column white matter showed similar qMT derived values in healthy controls, but significantly decreased macromolecular fraction (M_{ob}) in the dorsal column of AMN males. The results presented here may prove to be a benchmark for future spinal cord qMT studies at higher field and in different diseases.

It is convenient to assume that the spinal cord WM is similar to that of the brain. Morphologically, spinal cord WM consists of densely packed fiber bundles and is most similar to cerebral WM found in structures such as the internal capsule and corpus callosum (23). While few reports are given on the qMT derived metrics of these fiber pathways, the qMT derived parameters (M_{ob}, T_{2b}) of the lateral and dorsal column white matter in healthy controls fall within the range of reported values (14–16,24,25) for frontal WM: M_{ob} = 9–15%, T_{2b} = 9–12 μs (16,26). The variability and apparent discrepancy between the rate of MT exchange, R, reported here and elsewhere in the literature for brain and ex vivo tissue, can be accounted for by the difficulty with which R can be evaluated from a single power MT experiment (22). Similarly, spinal cord GM is similar to deep gray matter of the basal ganglia (e.g., caudate nucleus, putamen) and the qMT parameters derived here fall within published values for general, cerebral GM:

Table 1
qMT Parameters Derived From a Two-Pool Model Fit to the Acquired MTw z-Spectra for Cervical Spinal Cord White and Gray Matter*

	R (Hz)			M_{ob} (%)			T_{2b} (μs)		
	Lateral	Dorsal	GM	Lateral	Dorsal	GM	Lateral	Dorsal	GM
Control	52 ± 8	63 ± 14	67 ± 12	13 ± 2	15 ± 2	8 ± 2	9 ± 2	8 ± 1	9 ± 2
X-ALD Female									
ALD1	44 ± 21	76 ± 16	67 ± 14	13 ± 3	13 ± 2	5 ± 1	7 ± 1	10 ± 1	16 ± 2
ALD2	60 ± 30	66 ± 19	62 ± 27	16 ± 5	11 ± 6	6 ± 1	5 ± 3	17 ± 10	12 ± 8
ALD3	60 ± 20	67 ± 12	42 ± 29	13 ± 4	7 ± 1	7 ± 2	8 ± 4	14 ± 2	9 ± 1
ALD4	56 ± 20	19 ± 8	39 ± 18	7 ± 1	15 ± 2	7 ± 1	11 ± 3	4 ± 1	10 ± 2
ALD5	72 ± 22	53 ± 29	54 ± 23	10 ± 1	14 ± 3	9 ± 1	8 ± 1	5 ± 1	8 ± 1
Mean	58 ± 13	56 ± 22	53 ± 12	12 ± 4	12 ± 3	7 ± 1	8 ± 3	10 ± 6	11 ± 3
AMN Male									
AMN1	54 ± 40	60 ± 29	71 ± 8	11 ± 1	9 ± 1	5 ± 1	11 ± 2	5 ± 1	12 ± 2
AMN2	53 ± 25	53 ± 30	59 ± 27	11 ± 2	14 ± 3	7 ± 1	6 ± 1	4 ± 1	8 ± 1
AMN3	73 ± 19	66 ± 20	71 ± 42	11 ± 2	6 ± 1	6 ± 1	9 ± 1	9 ± 1	13 ± 1
AMN4	61 ± 34	56 ± 21	39 ± 21	13 ± 2	8 ± 1	15 ± 5	10 ± 2	9 ± 1	4 ± 2
Mean	61 ± 12	59 ± 6	60 ± 15	11 ± 2	9 ± 3	8 ± 5	9 ± 2	7 ± 3	9 ± 4

*White matter ROIs were taken from lateral and dorsal columns and gray matter taken from lateral/dorsal horn; both at the level of C2. R is the rate of MT exchange (in Hz), M_{ob} is the fraction of semisolid spins, and T_{2b} is the transverse relaxation time of the semisolid spins.

M_{ob} = 6–11%, T_{2b} = 9–12 μs. This indicates that, for healthy populations, the similarity between the spinal cord and brain tissues can be safely assumed.

Pathologically, AMN is unique in that it is a disabling spinal cord disease marked by distal axonopathy and concomitant demyelination of the cervical dorsal columns, but little or no inflammatory component. In agreement with histopathology, we found that in the dorsal column, the fraction of bound protons was decreased in AMN and X-ALD heterozygote patients. It was also observed that the lateral columns show little difference in the derived metrics for all groups studied, which seems to indicate the lack of tissue involvement in these columns in the cervical cord.

An interesting finding was that there was a wide range of variability in the macromolecular transverse relaxation time, T_{2b}, and the rate of MT exchange, R, in the dorsal column of the X-ALD females. Interestingly, closer examination revealed that three of five of the females (Table 1) showed T_{2b} similar to reported literature values for healthy tissue (T_{2b} range = 10–16 μs; mean = 13.7 μs), while 2/5 X-ALD females showed dramatically reduced T_{2b} (T_{2b} range = 3.8–4.6 μs; mean = 4.2 μs). In these same patients, an increase in the rate of MT exchange was also observed. Even though preliminary, these results are exciting and may potentially relate to the fact that the clinical disability in X-ALD heterozygotes varies widely as well. Furthermore, in comparison with other WM diseases, changes in the qMT-derived parameters were less obvious and were not accompanied by concomitant T_1/T_2-weighted signal abnormalities. Because there were no apparent signal abnormalities in T_1- or T_2-weighted images, we did not compare these results with standard measures of myelin water relaxation (27). However, our results indicate that qMT may be capable of capturing subtle changes at the macromolecular level before overt T_1/T_2 relaxation aberrations.

In qMT studies of the brain, comparisons are often made with conventional imaging techniques. In the spinal cord, two model-independent methods exist to characterize the MT effect: the magnetization transfer ratio (MTR, 6) and the magnetization transfer normalized by cerebrospinal fluid (MTCSF, 20). The former is the standard method to quantify the MT effect because it removes contributions of T_1 and T_2 relaxation, while the latter, though compromised by T_1 and T_2 effects, has shown utility in quantifying the degree of pathology in AMN.

Examination of the dorsal column MTR taken at an offset frequency of 2.5 kHz reveals a significant, decreased signal in the AMN males (MTR (control) = 0.31 ± 0.02, MTR (AMN) = 0.28 ± 0.01; P = 0.015) when compared with the healthy control, but no difference was observed between the X-ALD heterozygotes and the healthy volunteers (MTR [control] = 0.31 ± 0.02, MTR [X-ALD] = 0.26 ± 0.07; P = 0.1) or between the X-ALD heterozygotes and the AMN males (P = 0.5). However, the dorsal column MTCSF taken at an offset frequency of 10 kHz shows a strong, significant difference in the MTCSF between controls and X-ALD heterozygotes (MTCSF [control] = 0.49 ± 0.03, MTCSF [X-ALD] = 0.58 ± 0.05; P = 0.004), controls and AMN males (MTCSF [control] = 0.49 ± 0.03, MTCSF [AMN] = 0.63 ± 0.05; $P < 0.001$), but not between X-ALD heterozygotes and AMN males (P = 0.2). This is in accord with previous findings (19,20).

While the single offset frequency MTCSF has been shown to be sensitive to the pathology in AMN, it is confounded by other contrast mechanisms (T_1 and T_2) and even potentially by T_{2b} which is the parameter ultimately defining the "width" of the MT effect and, therefore, the sensitivity of the MTCSF. MTR on the other hand, does not show the same degree of sensitivity as MTCSF or qMT derived metrics. In relationship to the qMT findings reported here, it is possible that the MTR shows no difference between healthy and diseased cords by virtue of low SNR rather than MT insensitivity. This is mitigated to a degree when doing qMT analysis because information from all offset frequencies is used to derive the individual metrics. The MTCSF does in fact show a difference between the diseased and healthy cords, which could in part be due to changes in spin density, which drives the macromolecular proton fraction observed by qMT.

It is prudent to mention some of the limitations of the methods used in this study. First, qMT calculations suffer from low SNR and, therefore, multiple slices of the spinal cord were averaged to achieve the necessary SNR for fitting. Because we applied this in AMN, a diffuse disease, we can assume that each slice at the cervical level will show similar degree of involvement without the loss of generality. Second, the fitting methods here were used with only one power of MT irradiation. It has been shown that better fitting and more robust estimates of the qMT parameters can be achieved when applying a global fit to multiple powers (22). However, analysis of the quality of fit shows that the fit to the z-spectra are quite good (χ^2 = 1.3 and not exceeding 1.6) as shown in Figure 2. Along a similar line, the estimated error per metric did not exceed 7%, which was calculated according to (22). Therefore, even at one power, the fit and resulting qMT-derived metrics show a high degree of reliability.

In this work, only a short section of the cervical spinal cord was chosen for further analysis, however the results can be interpreted as being representative of a much larger segment of the cord. The spinal cord is an essentially linear organ and changes in tissue morphology over the rostral–caudal direction are gradual. In the cervical level, superior to the branching of the brachial plexus, spinal cord WM and GM are known to differ only in shape rather than in composition. It is possible that future studies of the spinal cord at different levels (e.g., thoracic, lumbar, *conus medularis*) might reveal differences in qMT parameters as compared to this and previous works.

CONCLUSION

For the first time qMT derived metrics (M_{ob}, T_{2b}, and R) are reported in the human spinal cord in vivo. The ramification from such experiments is the ability to use qMT to assess and characterize spinal cord tissue in disease and health with the ultimate goal of understanding the underpinnings of tissue destruction caused by diseases such as multiple sclerosis, transverse myelitis, and spinal cord trauma.

ACKNOWLEDGMENTS

The authors thank Jonathan Farrell for insight into the project. Also, Terri Brawner, Kathleen Kahl, and Joe Gillen for their assistance in data acquisition and MR methodology. Dr. Peter van Zijl is a paid lecturer for Philips Medical Systems. This arrangement has been approved by Johns Hopkins University in accordance with its Conflict of Interest policies.

REFERENCES

1. Kucharczyk W, Macdonald PM, Stanisz GJ, Henkelman RM. Relaxivity and magnetization transfer of white matter lipids at MR imaging: importance of cerebrosides and pH. Radiology 1994;192:521–529.
2. Wolff SD, Balaban RS. Magnetization transfer contrast (MTC) and tissue water proton relaxation in vivo. Magn Reson Med 1989;10:135–144.
3. Barkovich AJ. Magnetic resonance techniques in the assessment of myelin and myelination. J Inherit Metab Dis 2005;28:311–343.
4. Catalaa I, Grossman RI, Kolson DL, Udupa JK, Nyul LG, Wei L, Zhang X, Polansky M, Mannon LJ, McGowan JC. Multiple sclerosis: magnetization transfer histogram analysis of segmented normal-appearing white matter. Radiology 2000;216:351–355.
5. Dousset V, Grossman RI, Ramer KN, Schnall MD, Young LH, Gonzalez-Scarano F, Lavi E, Cohen JA. Experimental allergic encephalomyelitis and multiple sclerosis: lesion characterization with magnetization transfer imaging. Radiology 1992;182:483–491.
6. Filippi M, Rocca MA. Magnetization transfer magnetic resonance imaging in the assessment of neurological diseases. J Neuroimaging 2004; 14:303–313.
7. Kabani NJ, Sled JG, Chertkow H. Magnetization transfer ratio in mild cognitive impairment and dementia of Alzheimer's type. Neuroimage 2002;15:604–610.
8. Kalkers NF, Hintzen RQ, van Waesberghe JH, Lazeron RH, van Schijndel RA, Ader HJ, Polman CH, Barkhof F. Magnetization transfer histogram parameters reflect all dimensions of MS pathology, including atrophy. J Neurol Sci 2001;184:155–162.
9. Reich DS, Smith SA, Jones CK, Zackowski KM, van Zijl PC, Calabresi PA, Mori S. Quantitative characterization of the corticospinal tract at 3T. AJNR Am J Neuroradiol 2006;27:2168–2178.
10. Smith SA, Farrell JA, Jones CK, Reich DS, Calabresi PA, van Zijl PC. Pulsed magnetization transfer imaging with body coil transmission at 3 Tesla: feasibility and application. Magn Reson Med 2006;56:866–875.
11. Bryant RG. The dynamics of water-protein interactions. Annu Rev Biophys Biomol Struct 1996;25:29–53.
12. Gochberg DF, Gore JC. Quantitative imaging of magnetization transfer using an inversion recovery sequence. Magn Reson Med 2003;49:501–505.
13. Harrison R, Bronskill MJ, Henkelman RM. Magnetization transfer and T2 relaxation components in tissue. Magn Reson Med 1995;33:490–496.
14. Sled JG, Pike GB. Quantitative imaging of magnetization transfer exchange and relaxation properties in vivo using MRI. Magn Reson Med 2001;46:923–931.
15. Stanisz GJ, Kecojevic A, Bronskill MJ, Henkelman RM. Characterizing white matter with magnetization transfer and T2. Magn Reson Med 1999;42:1128–1136.
16. Yarnykh VL. Pulsed Z-spectroscopic imaging of cross-relaxation parameters in tissues for human MRI: theory and clinical applications. Magn Reson Med 2002;47:929–939.
17. Moser HW, Moser AB, Naidu S, Bergin A. Clinical aspects of adrenoleukodystrophy and adrenomyeloneuropathy. Dev Neurosci 1991;13: 254–261.
18. Powers JM, DeCiero DP, Ito M, Moser AB, Moser HW. Adrenomyeloneuropathy: a neuropathologic review featuring its noninflammatory myelopathy. J Neuropathol Exp Neurol 2000;59:89–102.
19. Fatemi A, Smith SA, Dubey P, Zackowski KM, Bastian AJ, van Zijl PC, Moser HW, Raymond GV, Golay X. Magnetization transfer MRI demonstrates spinal cord abnormalities in adrenomyeloneuropathy. Neurology 2005;64:1739–1745.
20. Smith SA, Golay X, Fatemi A, Jones CK, Raymond GV, Moser HW, van Zijl PC. Magnetization transfer weighted imaging in the upper cervical spinal cord using cerebrospinal fluid as intersubject normalization reference (MTCSF imaging). Magn Reson Med 2005;54:201–206.
21. Morrison C, Stanisz GJ, Henkelman R. Modeling magnetization transfer for biological-like systems using a semi-solid pool with a super-Lorentzian lineshape and dipolar reservoir. J Magn Reson B 1995;108:103–113.
22. Portnoy S, Stanisz GJ. Modeling pulsed magnetization transfer. Magn Reson Med 2007;58:144–155.
23. Kandel E, Schwartz JH, Jessell TM. Principles of neural science. New York: McGraw-Hill; 2000.
24. Ropele S, Seifert T, Enzinger C, Fazekas F. Method for quantitative imaging of the macromolecular 1H fraction in tissues. Magn Reson Med 2003;49:864–871.
25. Stanisz GJ, Odrobina EE, Pun J, Escaravage M, Graham SJ, Bronskill MJ, Henkelman RM. T1, T2 relaxation and magnetization transfer in tissue at 3T. Magn Reson Med 2005;54:507–512.
26. Sled JG, Pike GB. Quantitative interpretation of magnetization transfer in spoiled gradient echo MRI sequences. J Magn Reson 2000;145:24–36.
27. Laule C, Vavasour IM, Kolind SH, Traboulsee AL, Moore GR, Li DK, Mackay AL. Long T2 water in multiple sclerosis: what else can we learn from multi-echo T2 relaxation? J Neurol 2007;254:1579–1587.